



## Sr-Nd-Hf isotopes along the Pacific Antarctic Ridge from 41 to 53°S

Cédric Hamelin,<sup>1,2</sup> Laure Dosso,<sup>3</sup> Barry Hanan,<sup>4</sup> Jean-Alix Barrat,<sup>1</sup> and Hélène Ondréas<sup>5</sup>

Received 19 February 2010; revised 1 April 2010; accepted 9 April 2010; published 19 May 2010.

[1] Major, trace element and Sr-Nd-Hf isotope data in basalts collected along the Pacific-Antarctic Ridge (PAR) axis between 53 and 41°S, far from any hotspot influence, reveal tight coherent geochemical variations within the depleted MORB mantle. All samples are located below the Pacific reference line defining two sub-oceanic mantle domains on each side of the Easter microplate. The data extend the PAR 66–53°S field towards more radiogenic Sr (0.70264), less radiogenic Nd ( $\epsilon = 7.7$ ) and Hf ( $\epsilon = 11.4$ ) values. The along ridge geochemical variability is closely related to the morphological segmentation of the ridge. Anomalous geochemical features are attributed to the atypical morphology of two segments due to the presence of off-axis magmatism. The first order ridge discontinuity defined by the Menard transform fault separates two slightly different mantle domains, each with its own history. **Citation:** Hamelin, C., L. Dosso, B. Hanan, J.-A. Barrat, and H. Ondréas (2010), Sr-Nd-Hf isotopes along the Pacific Antarctic Ridge from 41 to 53°S, *Geophys. Res. Lett.*, 37, L10303, doi:10.1029/2010GL042979.

### 1. Introduction

[2] Mid-Ocean Ridge Basalts (MORB) geochemical heterogeneity has been often documented and has led to question the widespread concept of a geochemically uniform depleted MORB mantle (DMM) [Hofmann, 2003]. The description of a ridge geochemical feature in relation with its physical (morphological, structural and geophysical) parameters generally leads to a discussion of the depleted mantle structure and processes (cf. review paper by Hofmann [1997]). The studied section of the Pacific-Antarctic ridge is devoid of plume influence. It allows a detailed description of the different scales of heterogeneity present in the south sub-Pacific depleted mantle.

[3] In 1999, a large scale geochemical division of the Pacific mantle was proposed, based on available Mid-Ocean Ridge Basalt data from the Pacific ridge together with data from samples collected during the PACANTARCTIC1 cruise between 53 and 66°S [Vlastélic et al., 1999]. The boundary was identified at the latitude of the Easter Island microplate. Yet there was still a large sampling gap along the ridge axis between 53 and 41°S. Therefore this became

one of the main objectives of the PACANTARCTIC2 cruise, which took place during the austral summer 2004–05 [Dosso et al., 2005; Klingelhoefer et al., 2006]. This paper first describes the geological context of the studied ridge section, and then presents the geochemical results of the cruise with major element data, trace element and Sr-Nd-Hf isotopic data from axial samples collected between 41 and 53°S, on each side of Menard Transform Fault (TF).

### 2. Geological Setting and Sampling

[4] The Pacific-Antarctic Ridge (PAR), south of the Chile Triple Junction (Juan Fernandez microplate) at 35°S/110°W separates the Pacific plate from the Antarctic plate (Figure 1). The full spreading rate of the ridge increases from 54 mm/yr at 65°S to 74 mm/yr near Udintsev Transform Fault (TF) at 55°S, and to 100 mm/yr at 35°S. In conjunction, the ridge axis morphology changes from a valley at 65°S to a dome north of 60°S [Ondréas et al., 2001]. A large portion of this plate boundary, including major fracture zones, has been previously surveyed [Lonsdale, 1994; Cande et al., 1995] but only the southern section has been systematically sampled [Géli et al., 1997; Castillo et al., 1998; Vlastélic et al., 2000].

[5] The PACANTARCTIC2 cruise was a joint geophysical survey and geochemical sampling of the Pacific-Antarctic Ridge between 41°15'S and 52°45'S (Figure 1). This 1300 km-long ridge section is characterized by a dome shape axial morphology. It is segmented by the Menard TF near 50°S and by small non-transform offsets such as Overlapping Spreading Centers (OSC). The cruise imaged three segments south of the Menard TF (S1 to S3) and six segments north of it (N1 to N6). Segment morphology varies from a robust 12 km-wide dome to a narrower rise, 2 km in width. S2 and N2 are rather poorly defined and are seen as transitional ridge segments. The half spreading rate varies between 46 mm/yr at 52°S to 50 mm/yr at 42°S [Lonsdale, 1994] while the ridge bathymetry decreases from 2300 to 2500 m. Twenty four dredges were collected along axis at regular intervals (3 to 4 regularly spaced dredges per segment) and 19 dredges were collected off-axis. This paper reports only on results from axial samples. All dredges brought back aphyric samples except DR20, which is a plagioclase-phyric rock.

### 3. Analytical Techniques and Results

[6] Major, trace element and isotope (Sr, Nd, Hf) data are presented in Table S1 of the auxiliary material.<sup>6</sup> Major element analyses were performed by ICP-AES at Brest following the method described by Cotten et al. [1995]. The relative standard deviations are less than 2%. Trace element

<sup>1</sup>Laboratoire Domaines Océaniques, UMR 6538, IUEM, UBO, Plouzané, France.

<sup>2</sup>Now at IPGP, Paris, France.

<sup>3</sup>Laboratoire Domaines Océaniques, UMR 6538, CNRS, IFREMER, Plouzané, France.

<sup>4</sup>Geological Sciences, San Diego State University, San Diego, California, USA.

<sup>5</sup>IFREMER, Plouzané, France.

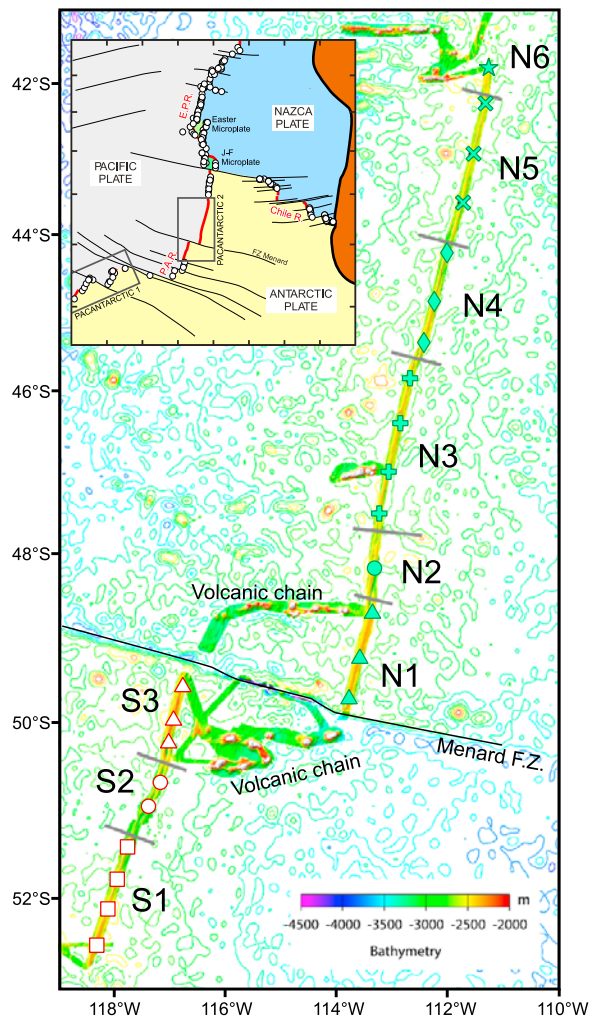


**Figure 1.** Sample location map. Segments are limited by overlapping spreading centers (OSC) marked by grey line segments. All symbols are specific to each segment and are kept the same in Figures 1–4. The insert shows the location map of the PACANTARCTIC 2 cruise with respect to the Pacific–Antarctic ridge axis and the main fracture zones. Opened circles indicate the location of PetDB samples.

analyses were performed by ICP-MS at Brest using Finnigan Element2 and the method described by *Barrat et al.* [1996]. Based on standard measurements and sample duplicates, trace element concentrations reproducibility is generally better than 5% [*Barrat et al.*, 2007]. For isotope analyses, the powder was further leached to remove seawater alteration. The Sr–Nd separations were done according to the procedure described by *Dosso et al.* [1993]. The Hf elution was performed using the protocol of *Blichert-Toft et al.* [1997] at SDSU. Sr and Nd were measured with a Finnigan MAT26x multicollector instrument (MAT261 upgraded by Spectromat). Hf isotope ratios were measured at San Diego State University using the Nu Plasma 1700. Standards NBS987 (Sr), JNdi-1 (for Nd) and JMC-475 (for Hf) analyzed during the sample measurement period gave values of  $0.710251 \pm 16$ ,  $0.512104 \pm 4$  and  $0.282160 \pm 10$  respectively.

[7] All but two dredges (namely DR06-1 and DR09-1) have negative loss of ignition reflecting the lack of alteration and the pristine nature of the samples. Nearly all samples are typical basalts and only the samples collected close to the Menard TF (DR09, DR20) or in the transitional ridge segments S2 and N2 (DR06, DR27) are slightly different and present higher alkali contents. The great majority of samples is geochemically homogeneous and present typical MORB patterns with a clear depletion in most light rare earth elements and in most cases a slight negative anomaly in Eu due to plagioclase fractionation. Concerning the isotopic measurements, all samples from the PACANTARCTIC2 cruise are located in the global MORB field and below the Pacific Reference Line (PRL) [*Vlastélic et al.*, 1999]. PAC2 data extend the PAR 66–53°S data field towards more radiogenic Sr (0.70264), less radiogenic Nd ( $\epsilon = 7.7$ ) and Hf ( $\epsilon = 11.4$ ) values.

[8] Major, trace element and Sr–Nd–Hf isotope data reveal tight and coherent geochemical variations along segments (Figure 2). Along axis geochemistry can be disturbed by local phenomena like the presence of nearby seamounts as seen in S2 and N2 (Figure 1) [*Briais et al.*, 2009]. These segments are the shortest and the less robust of the studied area. They are likely to erupt melts that are extracted over a restricted depth range as compared to melts from the ridge. Therefore melt mixing during extraction would be more limited than at the ridge, leading to larger trace element and isotope variation [*Stracke and Bourdon*, 2009]. S3 and N1 have directions that are perpendicular to the Menard TF but deviate from the main direction of the ridge. S2 and N2 accommodate this change. They can therefore be seen as atypical segments and transitional zones between a Menard related zone and the rest of the ridge, i.e. S1 on one side and N3–N6 on the other. This most likely reflects the resistance of the Menard transform fault to the latest kinematic movements [*Sahabi et al.*, 1996].

#### 4. Discussion

[9] The Menard transform fault (Figure 1) is a major geological feature, a first order discontinuity cutting across our study area. But does it also play a major geochemical role? Are there differences in the geochemical characteristics of samples on each side of the transform fault?

[10] Major elements plot along similar differentiation trends for all segments (see supplementary material). This underlines the first-order major element homogeneity of the mantle source and the similarities in the mineral assemblage involved in the crystallization process. It also suggests similarities in the physical conditions of the magmatic plumbing system of the studied ridge section. In the Sr–Nd or in the Nd–Hf plot (Figure 3), the PAC2 data define an elongated field extending the PAR 66–53°S data field towards more radiogenic Sr (0.70264), less radiogenic Nd ( $\epsilon = 7.7$ ) and Hf ( $\epsilon = 11.4$ ) values. In these representations, the least radiogenic Sr (and most radiogenic Nd and Hf) samples are found to the south of Menard TF whereas the most radiogenic ones are found to the north. Each side of the Menard TF can be represented as individual data fields, which partially overlap each other around 0.7025, 8.7 and 12.5. This slight isotopic difference has also been noted using helium isotopic ratios [*Moreira et al.*, 2008]. It has to

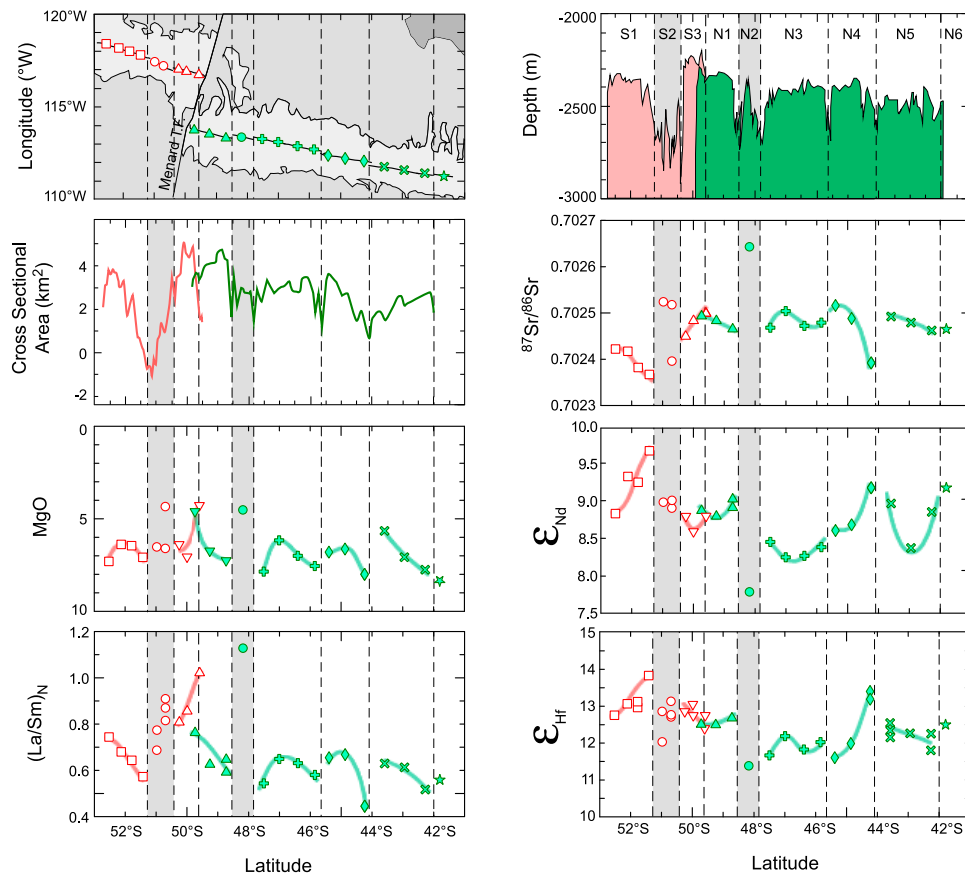


**Figure 2.** Along-axis variations of the ridge physical (cross sectional area, depth) and chemical (MgO, (La/Sm)<sub>N</sub>, Sr-Nd-Hf isotopic compositions) parameters. Dashed lines indicate the location of the overlapping spreading centers with a grey shade used for atypical segments S2 and N2.

be noted that it is of a much lower magnitude than the isotopic variations reported across the Australian-Antarctic Discordance [Christie, 1998; Hanan *et al.*, 2004] or along the Gakkel Ridge [Michael *et al.*, 2003; Goldstein *et al.*, 2008]. Could this slight isotopic difference between the north and south Menard TF also be identified using trace element ratios? A plot of <sup>87</sup>Sr/<sup>86</sup>Sr versus (La/Sm)<sub>N</sub> reveals two separate and sub-parallel linear trends (Figure 4). The two arrays are tightly linked to the geographical distribution of samples with respect to Menard TF. Excluding samples from atypical segments (S2 and N2), a regression calculation through each one of these 2 trends gives rather good regression coefficients *r* of 0.96 and 0.84 for the south and north part of the ridge respectively. For a given (La/Sm)<sub>N</sub>, the northern trend presents systematically more radiogenic Sr isotopic values than the southern trend. Their difference in <sup>87</sup>Sr/<sup>86</sup>Sr is significant, about 0.0001 at a constant (La/Sm)<sub>N</sub>. On each side of the TF, the observed trace element variation as well as the isotopic variability are comparable, suggesting comparable melt mixing during melt extraction [Stracke and Bourdon, 2010].

[11] Based on the incompatibility order of trace elements, it is interesting to point out that a plot of <sup>87</sup>Sr/<sup>86</sup>Sr versus (La/Sm)<sub>N</sub> is equivalent to a plot of <sup>87</sup>Sr/<sup>86</sup>Sr versus <sup>87</sup>Rb/<sup>86</sup>Sr, which is an isochron diagram. The correlations along the North and South segments are weaker in the isochron diagram, likely due to the greater sensitivity of the elements Rb and Sr to alteration and fractional crystalliza-

tion compared to La/Sm. It is interesting to note that these correlations are observed here in a geochemically depleted environment, whereas in most cases, they are described in oceanic environment with the nearby presence of enriched basalts [Zindler *et al.*, 1984; Dosso *et al.*, 1999; Donnelly *et al.*, 2004]. As underlined by many authors, the slopes of these “mantle isochrons” do not date a specific event [e.g., Donnelly *et al.*, 2004; Rudge, 2006, and references therein]. Rather they are the result of a combination of two competing processes: one, which creates heterogeneities through time (i.e., chemical fractionations during subduction and crust extraction) and the other one, which tends to continuously homogenize the mantle (i.e., convection). Therefore, the slope is a function of physical characteristics of the reservoir such as mixing time, residence time and a parameter that accounts for the increase in the dispersion of the trace element ratio due to petrogenetic processes [Allègre, 2005]. The fact that the correlations on each side of the Menard TF are subparallel strongly suggests that each of the two mantle domains present comparable physical parameters. Each trend reflects individual mantle domains, each with their own proportions of enriched material, on each side of Menard TF. This leads to questions like: why does such mantle domain boundary occur at a tectonic boundary? Could it represent the location of a deep ‘impediment’ to flow in the upper mantle that originates from the continents during basin formation? To study the limit between the two domains, we can examine the dredges closest to the fracture,

namely DR09 and DR20 from S3 and N1 respectively. Their major element contents indicate evolved characteristics (Figure 2). This is coherent with their higher rare earth concentrations, with patterns that display europium anomalies indicative of plagioclase fractionation. Their  $(\text{La}/\text{Sm})_N$  is also higher than further away along the ridge without a significant change in their isotopic ratios (Figures 2 and 4). These chemical features could be caused by coupled effect of melting and crystal fractionation close to the transform fault. Lower upwelling rates and mantle temperatures near the rigid boundary create perturbations in melt production, which explains the evolved character of the erupted magmas [Morgan and Forsyth, 1988]. Similar chemical features due to the Transform Fault Effect [Langmuir and Bender, 1984] are described along the southern part of the PAR and shown in Figure 3 of Vlastélic *et al.* [2000].

## 5. Conclusion

[12] The data presented above, from a ridge section devoid of hotspot influence, emphasize the depletion and first order homogeneity commonly found in MORB. In spite of this regional homogeneity, the data reveal tight geochemical variations at the local segment scale. Moreover, the first isotopic data along this ridge section extend the PAR 66–53°S data field towards more radiogenic Sr (0.70264), less radiogenic Nd ( $\epsilon = 7.7$ ) and Hf ( $\epsilon = 11.4$ )

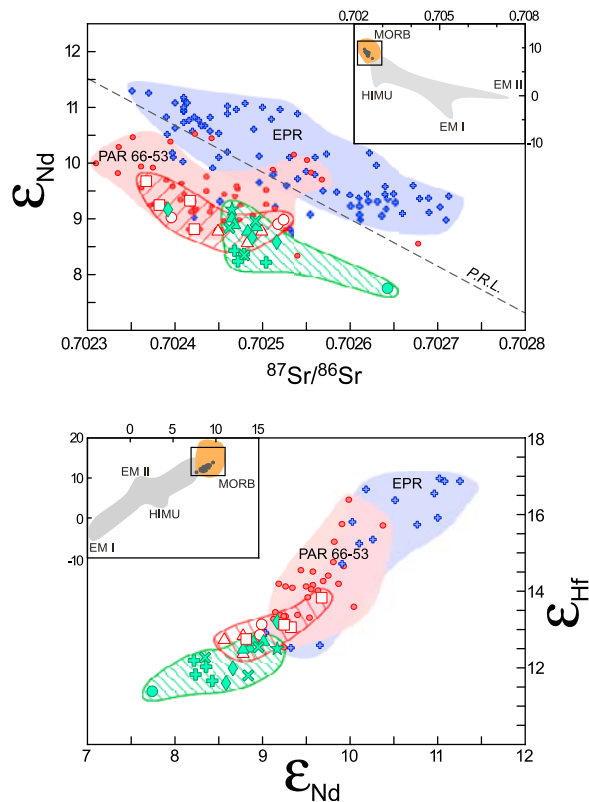


**Figure 3.** Sr-Nd and Nd-Hf isotopic plot of PAC2 data as compared to data from the EPR (crosses) and the PAR from 66 to 53°S (small circles). Two hatched fields define the PAC2 data for samples located north and south of Menard TF. The dashed line in the Sr-Nd plot is the Pacific Reference Line (PRL) as defined by Vlastélic *et al.* [1999].

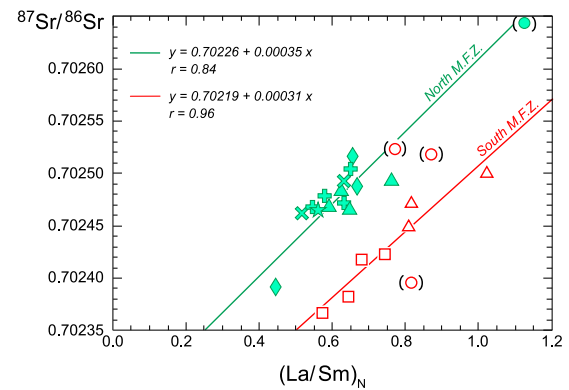


**Figure 4.** Sr isotopic composition versus  $(\text{La}/\text{Sm})_N$ . Regression lines are calculated through the two groups of samples located south (red line) and north (green line) of Menard TF.

values. In this depleted mantle environment, along axis slight but systematic geochemical variations can be disturbed by local phenomena like the presence of atypical segments, likely related to nearby seamounts as seen in S2 and N2. The Menard TF, which is the major geological feature along the studied area, appears to separate two mantles with slightly different geochemical characteristics. The northern part presents systematically more radiogenic Sr isotopic values for a given  $(\text{La}/\text{Sm})_N$  than the southern section. This result is in good agreement with the isotopic difference observed in He isotopic ratios [Moreira *et al.*, 2008] and confirms that the Menard TF acts as a discontinuity between two slightly different mantle domains.

[13] **Acknowledgments.** This work was funded by CNRS/INSU and IFREMER. We wish to thank the Captain, Michel Houmard, and the Crew of R/V L'Atalante for their efforts and expertise during the PACANTARCTIC2 cruise. This Hf isotope work was supported by NSF grants to Barry Hanan. We thank Joan Miller for technical assistance at SDSU. We acknowledge Manuel Moreira and two anonymous reviewers for their valuable comments. We also want to thank Jo Cotten (ICP-AES) and Joël Etoubleau (XRF) for their careful analytical work.

## References

- Allègre, C. J. (2005), *Géologie Isotopique*, 492 pp., Belin, Paris.
- Barrat, J.-A., F. Keller, J. Amossé, R. N. Taylor, R. W. Nesbitt, and T. Hirata (1996), Determination of rare earth elements in sixteen silicate reference samples by ICP-MS after Tm addition and ion exchange separation, *Geostand. NewsL.*, 20(1), 133–139, doi:10.1111/j.1751-908X.1996.tb00177.x.
- Barrat, J.-A., A. Yamauchi, R. C. Greenwood, M. Bohn, J. Cotten, M. Benoit, and I. A. Franchi (2007), The Stannern trend eucrites: Contamination of main group eucritic by crustal partial melts, *Geochim. Cosmochim. Acta.*, 71, 4108–4124, doi:10.1016/j.gca.2007.06.001.
- Blichert-Toft, J., C. Chauvel, and F. Albarède (1997), Separation of Hf and Lu for high-precision isotope analysis of rock samples by magnetic sector-multiple collector ICP-MS, *Contrib. Mineral. Petrol.*, 127(3), 248–260, doi:10.1007/s004100050278.
- Briais, A., H. Ondréas, F. Klingelhoefer, L. Dosso, C. Hamelin, and H. Guillou (2009), Origin of volcanism on the flanks of the Pacific-Antarctic ridge between 41°30'S and 52°S, *Geochem. Geophys. Geosyst.*, 10, Q09001, doi:10.1029/2008GC002350.
- Cande, S. C., C. A. Raymond, J. Stock, and W. F. Haxby (1995), Geophysics of the Pitman fracture zone and Pacific-Antarctic plate motions during the Cenozoic, *Science*, 270, 947–953, doi:10.1126/science.270.5238.947.
- Castillo, P. R., J. Natland, Y. Niu, and P. F. Lonsdale (1998), Sr, Nd and Pb isotopic variation along the Pacific-Antarctic risedest, 53–57°S: Implications for the composition and dynamics of the South Pacific upper mantle, *Earth Planet. Sci. Lett.*, 154, 109–125, doi:10.1016/S0012-821X(97)00172-6.

- Christie, D. M., B. P. West, D. G. Pyle, and B. B. Hanan (1998), Chaotic topography, mantle flow and mantle migration in the Australian–Antarctic discordance, *Nature*, *394*, 637–644, doi:10.1038/29226.
- Cotten, J., A. Le Dez, M. Bau, M. Caroff, R. Maury, P. Dulski, S. Fourcade, M. Bohn, and R. Brousse (1995), Origin of anomalous rare Earth element and yttrium enrichments in subaerially exposed basalts: evidence from French Polynesia, *Chem. Geol.*, *119*, 115–138, doi:10.1016/0009-2541(94)00102-E.
- Donnelly, K. E., S. L. Goldstein, C. H. Langmuir, and M. Spiegelman (2004), Origin of enriched ocean ridge basalts and implications for mantle dynamics, *Earth Planet. Sci. Lett.*, *226*, 347–366, doi:10.1016/j.epsl.2004.07.019.
- Dosso, L., H. Bougault, and J. L. Joron (1993), Geochemical morphology of the North Mid-Atlantic Ridge, 10°–24°N: Trace element–isotopes complementarity, *Earth Planet. Sci. Lett.*, *120*, 443–462, doi:10.1016/0012-821X(93)90256-9.
- Dosso, L., H. Bougault, C. Langmuir, C. Bollinger, O. Bonnier, and J. Etoubleau (1999), The age and distribution of mantle heterogeneity along the Mid-Atlantic Ridge (31–41°N), *Earth Planet. Sci. Lett.*, *170*, 269–286, doi:10.1016/S0012-821X(99)00109-0.
- Dosso, L., H. Ondréas, A. Briais, P. Fernagu, G. Floch, C. Hamelin, B. B. Hanan, F. Klingelhoefer, M. Moreira, and A. Normand (2005), The Pacific–Antarctic Ridge between 41°15′S and 52°45′S: Survey and sampling during the PACANTARCTIC2 cruise, *InterRidge News*, *14*, 1–4.
- Géli, L., et al. (1997), Evolution of the Pacific–Antarctic Ridge south of the Udintsev fracture zone, *Science*, *278*, 1281–1284, doi:10.1126/science.278.5341.1281.
- Goldstein, S. L., G. Soffer, C. H. Langmuir, K. A. Lehnert, D. W. Graham, and P. J. Michael (2008), Origin of a “Southern Hemisphere” geochemical signature in the Arctic upper mantle, *Nature*, *453*, 89–93, doi:10.1038/nature06919.
- Hanan, B. B., J. Blichert Toft, D. G. Pyle, and D. M. Christie (2004), Contrasting origins of the upper mantle revealed by hafnium and lead isotopes from the Southeast Indian Ridge, *Nature*, *432*, 91–94, doi:10.1038/nature03026.
- Hofmann, A. W. (1997), Mantle geochemistry: The message from oceanic volcanism, *Nature*, *385*, 219–229, doi:10.1038/385219a0.
- Hofmann, A. W. (2003), Sampling mantle heterogeneity through oceanic basalts: Isotopes and trace elements, in *Treatise on Geochemistry*, vol. 2, *The Mantle and the Core*, edited by H. Holland and K. K. Turekian, pp. 1–44, Elsevier, Oxford, U. K.
- Klingelhoefer, F., H. Ondréas, A. Briais, C. Hamelin, and L. Dosso (2006), New structural and geochemical observations from the Pacific–Antarctic Ridge between 52°45′S and 41°15′S, *Geophys. Res. Lett.*, *33*, L21312, doi:10.1029/2006GL027335.
- Langmuir, C. H., and J. F. Bender (1984), The geochemistry of oceanic basalts in the vicinity of transform faults: observations and implications, *Earth Planet. Sci. Lett.*, *69*, 107–127, doi:10.1016/0012-821X(84)90077-3.
- Lonsdale, P. (1994), Geomorphology and structural segmentation of the crest of the southern (Pacific–Antarctic) East Pacific Rise, *J. Geophys. Res.*, *99*, 4683–4702, doi:10.1029/93JB02756.
- Michael, P. J., et al. (2003), Magmatic and amagmatic seafloor generation at the ultraslow-spreading Gakkel Ridge, *Arctic Ocean*, *Nature*, *423*, 956–961, doi:10.1038/nature01704.
- Moreira, M., L. Dosso, and H. Ondréas (2008), Helium isotopes on the Pacific–Antarctic Ridge (52.5–41.5°S), *Geophys. Res. Lett.*, *35*, L10306, doi:10.1029/2008GL033286.
- Morgan, J. P., and D. W. Forsyth (1988), Three-dimensional flow and temperature perturbations due to a transform offset: Effects on oceanic crustal and upper mantle structure, *J. Geophys. Res.*, *93*, 2955–2966, doi:10.1029/JB093iB04p02955.
- Ondréas, H., D. Aslanian, L. Géli, J.-L. Olivet, and A. Briais (2001), Variations in axial morphology, segmentation, and seafloor roughness along the Pacific–Antarctic Ridge between 56°S and 66°S, *J. Geophys. Res.*, *106*(B5), 8521–8546, doi:10.1029/2000JB900394.
- Rudge, J. F. (2006), Mantle pseudo-isochrons revisited, *Earth Planet. Sci. Lett.*, *249*, 494–513, doi:10.1016/j.epsl.2006.06.046.
- Sahabi, M., L. Géli, J. L. Olivet, L. Gilgcapar, G. Roullet, H. Ondréas, P. Beuzart, and D. Aslanian (1996), Morphological reorganization within the Pacific–Antarctic discordance, *Earth Planet. Sci. Lett.*, *137*, 157–173, doi:10.1016/0012-821X(95)01185-K.
- Stracke, A., and B. Bourdon (2009), The importance of melt extraction for tracing mantle heterogeneity, *Geochim. Cosmochim. Acta*, *73*, 218–238, doi:10.1016/j.gca.2008.10.015.
- Vlastélic, I., D. Aslanian, L. Dosso, H. Bougault, J. L. Olivet, and L. Géli (1999), Large-scale chemical and thermal division of the Pacific mantle, *Nature*, *399*, 345–350, doi:10.1038/20664.
- Vlastélic, I., L. Dosso, H. Bougault, D. Aslanian, L. Géli, J. Etoubleau, M. Bohn, J.-L. Joron, and C. Bollinger (2000), Chemical systematics of an intermediate spreading ridge: The Pacific–Antarctic Ridge between 56°S and 66°S, *J. Geophys. Res.*, *105*, 2915–2936, doi:10.1029/1999JB900234.
- Zindler, A., H. Staudigel, and R. Batiza (1984), Isotope and trace element geochemistry of young Pacific Seamounts: Implications for the scale of upper mantle heterogeneity, *Earth Planet. Sci. Lett.*, *70*, 175–195, doi:10.1016/0012-821X(84)90004-9.

J.-A. Barrat, Laboratoire Domaines Océaniques, UMR 6538, IUEM, UBO, Place Nicolas Copernic, F-29280 Plouzané CEDEX, France. (barrat@univ-brest.fr)

L. Dosso, Laboratoire Domaines Océaniques, UMR 6538, CNRS, IFREMER, BP70, F-29280 Plouzané CEDEX, France. (laure.dosso@univ-brest.fr)

C. Hamelin, IGP, 4 Place Jussieu, F-75252 Paris CEDEX 05, France. (hamelin@ipgp.fr)

B. Hanan, Geological Sciences, San Diego State University, 5500 Campanile Dr., San Diego, CA 92182-1020, USA. (bhanan@mail.sdsu.edu)

H. Ondréas, IFREMER, BP70, F-29280 Plouzané CEDEX, France. (helene.ondreas@ifremer.fr)